Method of Phase Diversity in Multi-aperture Systems Utilizing Individual Sub-aperture Control

Matthew R. Bolcar* and James R. Fienup
The Institute of Optics, University of Rochester, Rochester, NY 14627

ABSTRACT

Multi-aperture systems allow a natural method of implementing phase diversity for the joint estimation of both pupil aberrations and an image of the object. Instead of creating diversity images by means of focus adjustments, one can actuate the individual sub-apertures of the system (e.g., with a piston phase) to introduce known phase diversity. Implementation of a nonlinear optimization routine is discussed. Through digital simulation, this paper investigates the performance of a sub-aperture piston diversity algorithm by tracking Strehl ratio and the probability and speed of convergence of the nonlinear optimization routine.

Keywords: Phase diversity, multi-aperture systems, unconventional imaging, Fourier transform spectroscopy

1. INTRODUCTION

For segmented or multi-aperture systems, a common problem is the alignment of segments or sub-apertures to the required precision. For space-based systems imaging extended objects, phase diversity[1,2,3,4] has emerged as a preferred method for sensing aberrations. With very little extra optical hardware, phase diversity can simultaneously recover information about the object and system aberrations such as pupil misalignments. A necessary trade-off is that phase diversity algorithms are typically computationally intensive. Conventional phase diversity is achieved by introducing a global focus error on a series of two or more defocused images. Using knowledge of the phase diversity, a nonlinear optimization algorithm iteratively adjusts an estimate of the system and object parameters to minimize an objective function.

In this study, we explore the application of a new form of phase diversity associated with multi-aperture telescope systems. In such systems, the necessary control over the path length of each individual sub-aperture allows a piston phase error to be introduced at the sub-apertures. In particular, the question of whether sub-aperture piston phase diversity provides an advantage over the conventional global focus diversity is addressed. In Sec. 2 we motivate the problem and in Sec. 3, briefly discuss the theory. In Secs. 4 and 5 we discuss the digital simulations and results, respectively. Conclusions are drawn in Sec. 6.

2. MOTIVATION

Sub-aperture piston diversity by itself provides some advantages over the conventional global focus diversity in a multi-aperture system. First, the lack of additional hardware is attractive. Since sub-aperture phase diversity does not require multiple separate image planes or defocusing optics, the cost and complexity of the system can be reduced.

A second major advantage of sub-aperture piston diversity is its easy integration with current studies involving Fourier Transform Imaging Spectroscopy (FTIS) with multi-aperture systems.[5] In such systems, the individual sub-apertures are pistoned with varying path delays to collect spectral information. These images can also be used for phase diversity; hence it is possible to use the images collected by FTIS without having to take any additional images or use any additional optical hardware whatsoever.

* bolcar@optics.rochester.edu; phone: 585-273-5991; fax: 585-244-4936

Unconventional Imaging, edited by Victor L. Gamiz, Paul S. Idell, Proc. of SPIE Vol. 5896, 58960G, (2005) · 0277-786X/05/$15 · doi: 10.1117/12.613257

In some implementations of focus diversity, only a small portion of the detector is devoted to collecting diversity images. This can prove troublesome at times when that section of the image plane corresponds to a low-contrast portion of the object. High contrast diversity images work better. The ability of sub-aperture piston phase diversity to utilize the entire image plane in diversity measurements is a third advantage. The probability of obtaining diversity images that correspond to a high contrast portion of the object are much higher.

One disadvantage of sub-aperture piston diversity as compared to conventional focus diversity is the inability to collect simultaneous diversity images. A consequence of this is a required time stability of the object being observed. In other words, the object or system aberrations can not be changing faster than the time it takes to collect all of the phase diversity images. This stability, however, is already required by the FTIS operation.

3. THEORY

Figure 1 shows a multi-aperture system. Optical trombones are needed to maintain equivalent path-lengths between the sub-apertures. They can also be used to introduce a known piston error, at individual or groups of sub-apertures, given by

$$\phi_p = \frac{4\pi}{\lambda}\Delta z_p \tag{1}$$

where λ is the wavelength, Δz_p is the mirror motion, p is the sub-aperture index, and the additional factor of 2 occurs since it is operating in reflection.

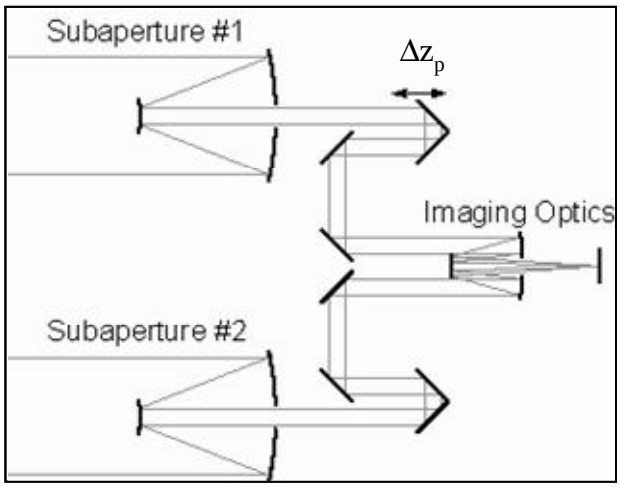

Figure 1 - Multi-aperture system

This known phase error adds to the unknown phase errors of the sub-apertures to give the total complex pupil function,

$$t(\xi) = \sum_{p=1}^{P} A_p(\xi)\exp\left\{ i\frac{2\pi}{\lambda}\left[2\Delta z_p + \sum_{j=1}^{J}\alpha_{p,j}Z_j(\xi)\right]\right\} \tag{2}$$

where $A_p(\xi)$ is the amplitude transmission function of the p^{th} sub-aperture, ξ is a 2-D aperture coordinate, and the unknown phase error has been expanded in a series of J basis functions, $Z_j(\xi)$, with coefficients $\alpha_{p,j}$ for the p^{th} sub-aperture. To implement the sub-aperture piston diversity, a series of images would be taken, each with a different amount of diversity, Δz_p, but the same unknown error. These images would then be used in a nonlinear optimization algorithm that minimizes an error metric. For this study, we have used the metric

$$E(f,\alpha) = \sum_{k=1}^{K}\sum_{x}\left[d_k(x) - f(x) * s_k(x)\right]^2 \tag{3}$$

where x is a 2-D image plane coordinate, $d_k(x)$ is the k^{th} detected diversity image, $f(x)$ is an estimate of the object, $s_k(x)$ is an estimate of the k^{th} incoherent point spread function (PSF) derived from an estimate of the aberrations, K is the number of diversity images. The in-line $*$ denotes convolution. Equivalently, in the Fourier domain, Eq. (3) can be written as

$$E(f,\alpha)=\sum_{k=1}^{K}\sum_{u}\left|D_k(u)-F(u)S_k(u)\right|^2 \tag{4}$$

where u is a 2-D Fourier domain coordinate, $D(u)$, $F(u)$ and $S_k(u)$ are the 2-D Fourier transforms of $d(x)$, $f(x)$ and $s_k(x)$, respectively. Note the $S_k(u)$ are the un-normalized optical transfer functions (OTFs) of the system.

In a monochromatic system, it is possible to use the Gonsalves method to simplify the error metric of Eq. (4) to a function of a single set of parameters.[2,6] This can greatly reduce the dimensionality of the search space. For example, if the set of object parameters, f, are $N\times N$ pixel values and the set of phase parameters, α, are J basis function coefficients over P sub-apertures, then it would be beneficial to remove the object parameters from the computation since N^2 may be on the order of tens of thousands to millions of pixels and $J\times P$ will typically be less than a few hundred coefficients. After performing the Gonsalves simplification, Eq. (4) becomes

$$E(\alpha)=\sum_{u}\sum_{k=1}^{K}\left|D_k(u)\right|^2-\sum_{u\in\chi_1}\frac{\left|\sum_{j=1}^{K}D_j(u)S_j^*(u)\right|^2}{\sum_{l=1}^{K}\left|S_l(u)\right|^2} \tag{5}$$

where we've introduced χ_1 as the set of pixel indices where the sum of the OTFs is not zero valued. It is now possible to optimize Eq. (5) with respect to the set of phase parameters, α. To further improve computational efficiency, we use an analytic gradient of this error metric to avoid having to compute finite differences during the optimization process. We can then use the estimate α in an image restoration algorithm such as a Wiener filter.

4. COMPUTER SIMULATIONS

A series of digital simulations was conducted to evaluate the performance of sub-aperture piston phase diversity and compare it with conventional global focus diversity. To take advantage of the Gonsalves simplification discussed earlier, the simulations were performed with monochromatic light, although this also means that 2π piston errors in the pupil cannot be detected. The system being modeled is a $f/30$, nine-aperture, circularly arrayed set of circular sub-apertures, as shown in Fig. 2.

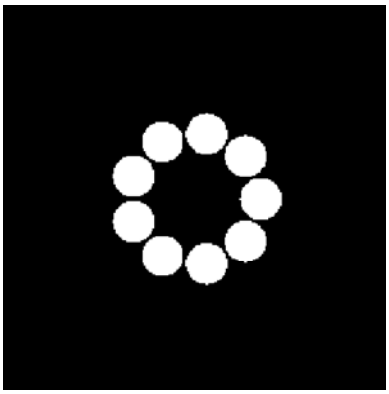

Figure 2 - System Pupil

The affects of noise are not explicitly investigated in this study; however, Gaussian noise was included to improve the realism of the simulations. An average pixel value of 20,000 and a standard deviation of 100 was assumed to give a signal-to-noise ratio of 200.

System performance was judged by the following criteria: accuracy of pupil phase estimates, the probability that the algorithm will converge to a faithful estimate, and the number of times the objective function and derivatives are evaluated before convergence is achieved.

The accuracy of the pupil phase estimates was determined by the Strehl ratio of the residual phase error

$$\phi_{res} = \phi_{true} - \phi_{est} \tag{6}$$

where ϕ_{true} is the true phase of the system pupil and ϕ_{est} is the phase diversity estimate. The Strehl ratio is then given by

$$\text{Strehl} = \frac{s_{res}(0)}{s_{ideal}(0)} \tag{7}$$

where $s_{res}(x, y)$ is the incoherent PSF of the pupil having the residual phase error given in Eq. (6) and $s_{ideal}(x)$ is the incoherent PSF of a perfectly aligned pupil, with no phase errors. Often, the phase diversity algorithm will estimate the correct pupil phase with additional global tip and tilt terms. Since these terms only introduce an arbitrary shift in the image plane, we do not care about them and therefore must remove them from $s_{res}(x)$ before calculating the Strehl ratio in Eq. (7). This was accomplished by performing a cross-correlation between $s_{res}(x)$ and $s_{ideal}(x)$ on a very fine sampling grid to determine the relative shift between them, and then appropriately shifting $s_{res}(x)$. A trial is said to have converged if the resulting Strehl ratio is greater than 90%, which corresponds to an RMS phase error of $\lambda/20$.

Figure 3 shows examples of the types of diversity being tested. In Fig. 3(a), an OPD has been introduced in four of the nine sub-apertures. In Fig. 3(b), the image plane has been shifted to introduce a global focus error.

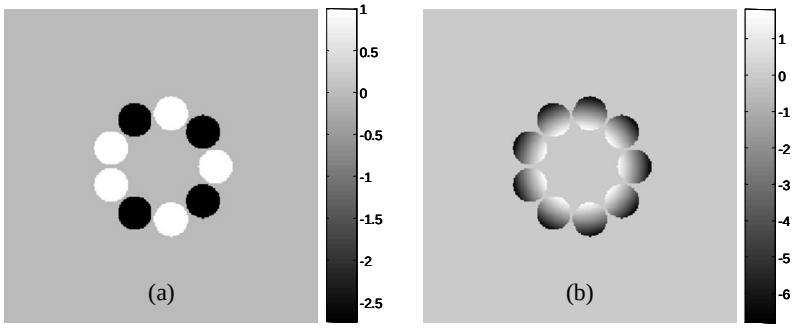

Figure 3 - Types of phase diversity: (a) sub-aperture piston diversity; (b) global focus diversity. A bias term was added to both plots to improve visualization. Color bar units are radians.

A series of Monte Carlo simulations was run. Twenty-five different realizations of approximately a quarter wave RMS of unknown phase error were simulated in the pupil. (Note: when we quote RMS phase values, the mean is subtracted from the phase before calculating the RMS.) For each realization of unknown error, four diversity images were simulated for each type of diversity. For the case of sub-aperture piston phase diversity, the amount of diversity in each image is determined by the peak-to-valley phase as given by Eq. (1). The equivalent RMS phase error in waves for the aperture arrangement in Fig. 3(a) is given by

$$\phi_{RMS}^{spp} = 0.4979\phi_{PV}^{spp} \tag{8}$$

where the superscript *spp* denotes sub-aperture piston phase diversity. The four diversity images then have RMS phase values in the set

$$\left\{ \phi_{RMS}^{spp} \quad \frac{\phi_{RMS}^{spp}}{2} \quad 0 \quad \frac{\phi_{RMS}^{spp}}{2} \right\}, \tag{9}$$

where the fourth phase diversity was the negative of the second. We then classify this set of diversity images by the maximum RMS diversity value in the set, ϕ_{RMS}^{spp}. For the case of global focus diversity over a filled circular aperture, the peak-to-valley phase error in waves is given by

$$\phi_{PV}^{foc} = \frac{1}{\lambda}\left[\frac{\Delta z}{8(f/\#)^2}\right] \tag{10}$$

where Δz is the amount by which the image plane has been shifted. The equivalent RMS phase error of the filled aperture is then given by

$$\phi_{RMS}^{foc} = 0.2887\phi_{PV}^{foc}. \tag{11}$$

For the aperture shown in Fig. 3(b), the RMS phase error in waves is given by

$$\phi_{RMS}^{foc,b} = 0.1862\phi_{PV}^{foc}, \tag{12}$$

a value less than that in Eq. (11) due to the pupil masking a significant portion of the phase error. The four diversity images then have RMS phase values in the set

$$\left\{ \phi_{RMS}^{foc,b} \quad \frac{\phi_{RMS}^{foc,b}}{2} \quad 0 \quad \frac{\phi_{RMS}^{foc,b}}{2} \right\} \tag{13}$$

where we again classify the set by the maximum RMS diversity value in the set, $\phi_{RMS}^{foc,b}$. Again, the fourth phase diversity was the negative of the second.

For each realization of unknown phase, there were 25 different realizations of an initial starting guess that were given to the nonlinear optimization routine. Each initial guess had a RMS phase error of approximately $\lambda/1000$. Figure 4 shows the scene that was used for the simulations as well as an example image that is blurred by the system OTF that includes a quarter wave RMS of unknown pupil aberrations.

Figure 4 - Left: Object scene used in simulations; Right: Image blurred by system OTF with 0.25 wave RMS unknown pupil aberration

5. RESULTS

The first result of interest is the accuracy of the pupil phase estimates. In Fig. 5, the average of the Strehl ratio for all 625 trials (25 realizations of unknown phase x 25 initial guesses) is plotted against the maximum amount of RMS phase diversity of the four diversity images, as given in Eqs. (9) and (13).

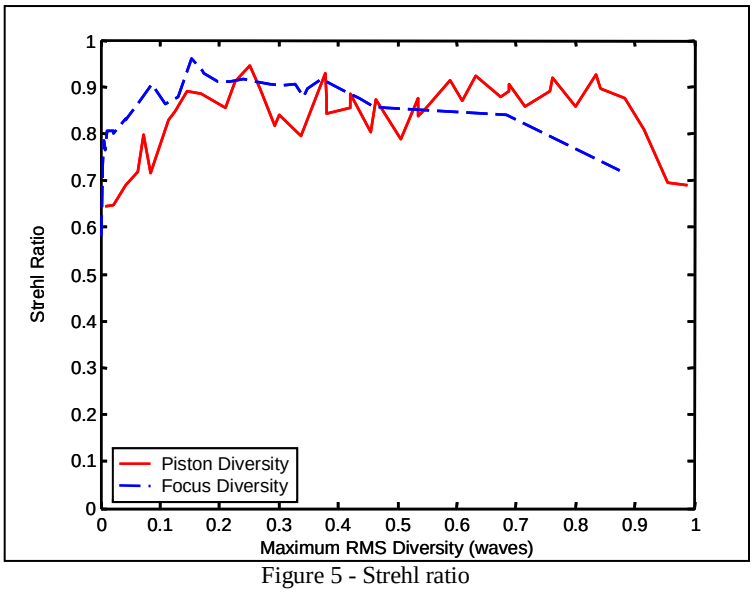

Figure 5 - Strehl ratio

The sub-aperture piston phase diversity exhibits a periodic nature, with a period of 0.9958 wave RMS of diversity. This is to be expected for monochromatic light, since a sub-aperture that is pistoned by a wavelength appears the same as a sub-aperture that has not been moved at all. The global focus diversity performance peaks for small amounts of diversity and then decreases as the amount of diversity becomes larger. This is due to large amounts of defocus reducing the MTF and spreading out the PSF. Beyond about 1 wave of maximum RMS phase diversity for the global focus diversity, the PSF becomes aliased and algorithm no longer converges. Note that neither type of diversity performs much worse than 70% Strehl. In cases when the algorithm did not converge, it usually results in a phase estimate near that of the original guess, which for each trial is about $\lambda/1000$ RMS. Therefore, the residual phase error given in Eq. (6) is about a quarter wave RMS which corresponds to a Strehl ratio of about 77%.

Figure 6 shows the convergence percentage for each type of diversity. Again, a trial is said to have converged if the Strehl ratio given by Eq. (7) is greater than 90%.

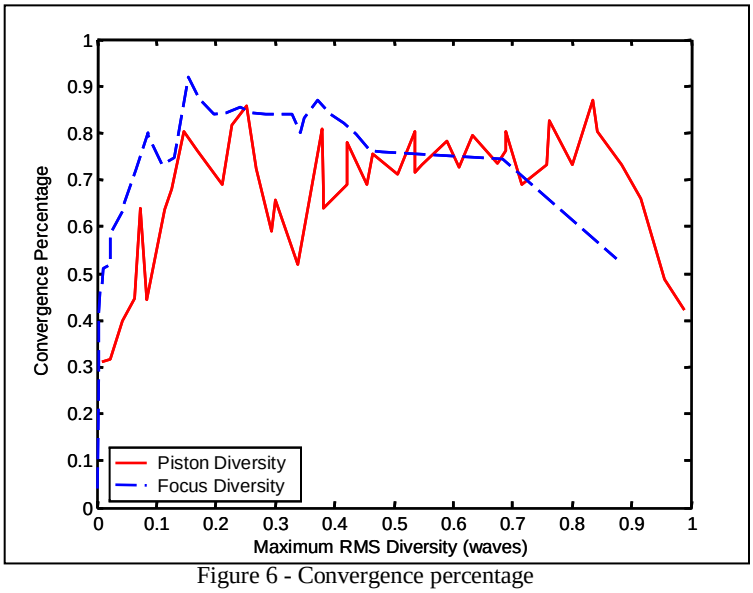

Figure 6 - Convergence percentage

For low amounts (0.1 to 0.75 waves RMS) of diversity, the sub-aperture piston phase diversity converged with similar probability as global focus diversity. However, for large amounts of diversity, the convergence of global focus diversity deteriorates. An important conclusion to draw is that for many cases, the convergence percentage is about 70%, which means that if a trial does not converge, it would be possible to reinitialize the optimization routine with several different starting guesses and eventually find an acceptable solution. The higher the convergence percentage, the fewer number of starting guesses would need to be made.

Finally, we consider the number of times the error metric and analytic gradients are calculated before the optimization routine converges to an acceptable solution. This is shown in Fig. 7.

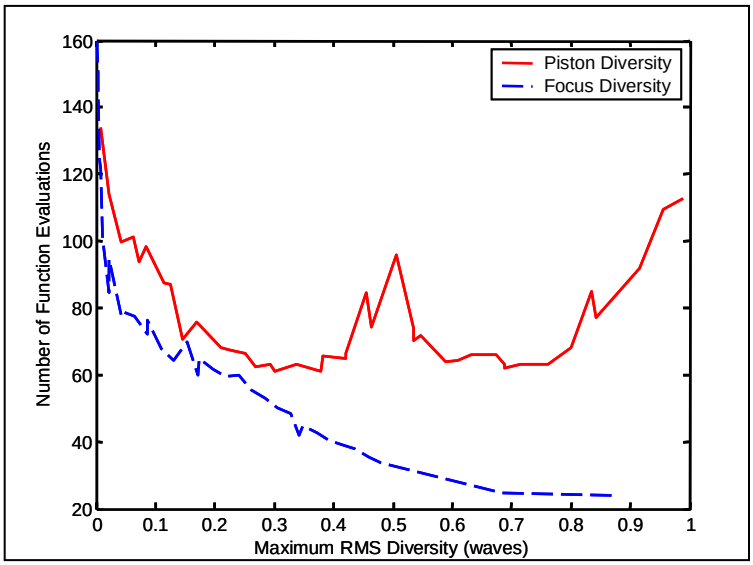

Figure 7 - Number of function evaluations before convergence

By this criterion, we see that global focus diversity outperforms piston diversity, especially for mild amounts of diversity. The periodic nature of the sub-aperture piston diversity can also be seen. The greater number of iterations at 1 wave RMS diversity corresponds to situations for which the sub-apertures in all four diversity images have been pistoned by an integer number of wavelengths, and therefore there is, effectively, no phase diversity. The smaller peak at half-wave RMS diversity values corresponds to situations for which in two of the four diversity images, the sub-apertures have been pistoned by an integer number of wavelengths and in the other two diversity images, the sub-apertures have been pistoned by a half-integer number of wavelengths. Therefore, the four diversity images are effectively reduced to two diversity images. While the algorithm still operates with only two diversity images, the performance is degraded somewhat.

In the real world, we would not have access to the true phase error in order to calculate the Strehl ratio as given by Eqs. (6) and (7). However, we do have access to the objective function value that is output by the nonlinear optimization routine. In Fig. 8, we plot the Strehl ratio (vertical axis) for each trial of a given amount of sub-aperture piston phase diversity against the normalized final objective function value (horizontal axis). Points with a Strehl ratio greater than 90% correspond to trials that converged. We see that for appropriate amounts of diversity (0.074 waves to 0.716 waves), we can clearly distinguish the trials that converged from those that did not, even if we only know the final objective function value given by the nonlinear optimization routine.

6. CONCLUSIONS

We have shown that sub-aperture piston phase diversity is a viable method of determining the phase errors of a multi-aperture pupil. Sub-aperture piston diversity performs almost as well as conventional global focus diversity with regards to phase error estimate accuracy and probability of convergence. From a computational standpoint, global focus diversity appears to require fewer iterations of the nonlinear optimization routine to converge. Piston diversity is especially advantageous in the context of an FTIS system.

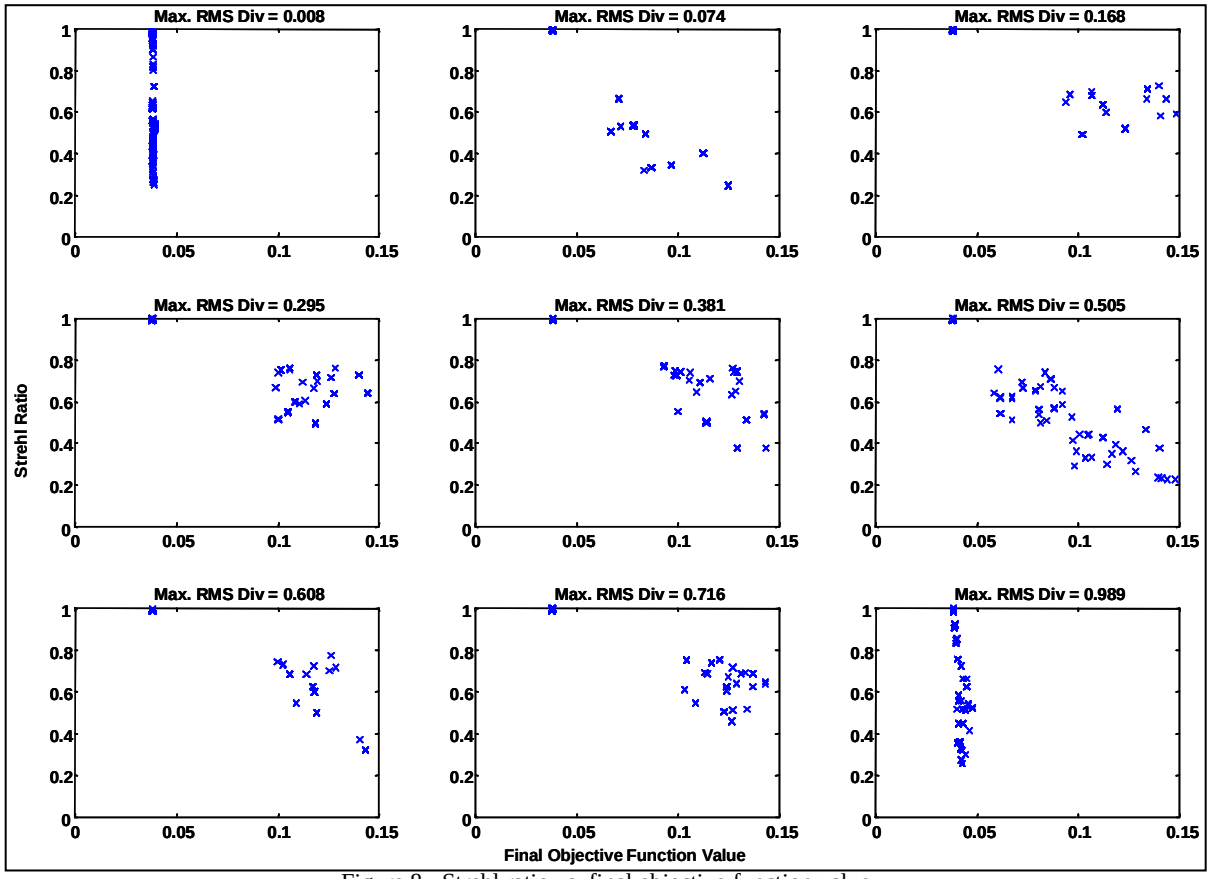

Figure 8 - Strehl ratio vs. final objective function value

ACKNOWLEDGMENTS

This work was supported by Lockheed Martin Corporation.

REFERENCES

1. R. G. Paxman and J. R. Fienup, "Optical misalignment sensing and image reconstruction using phase diversity," J. Opt. Soc. Am. A **5**, 914-923 (1988).
2. R.G. Paxman, T.J. Schulz and J.R. Fienup, "Joint estimation of object and aberrations by using phase diversity," J. Opt. Soc. Am. A **9,** 1072-1085 (1992).
3. J. Seldin, R. Paxman, V. Zarifis and R. Stone, "Closed-loop wavefront sensing for a sparse aperture multitelescope array using broadband phase diversity," Proc. SPIE **4091**, 48-63 (2000)
4. D. Carrara, B. Thelen and R. Paxman, "Aberration correction of segmented aperture telescopes by phase diversity," Proc. SPIE **4123**, 56-63 (2000).
5. S. T. Thurman and J. R. Fienup, "Multi-aperture Fourier transform imaging spectroscopy: theory and imaging properties," Opt. Exp. **13**, 2160-2175 (2005).
6. R. A. Gonsalves and R. Childlaw, "Wavefront sensing by phase retrieval," Proc. SPIE **207**, 32-39 (1979).